

Supporting Information

Sustainable nanocarriers fabricated by the dipeptide-based co-assemblies for enhancing the delivery and translocation of herbicide

Zirui Zheng, Ziyun Yang, Zehua Meng, Siyang Liu, Tianyue Wu, Chengyi He, Chenhui Zhang,
Chen Ma,* Yuxia Gao,* Fengpei Du*

Department of Applied Chemistry, College of Science, China Agricultural University, No. 2
Yuanmingyuan West Road, Haidian District, Beijing 100193, P. R. China

*Corresponding authors

E-mail address: machen@cau.edu.cn (C. Ma), gaoyuxia@cau.edu.cn (Y. Gao),
dufp@cau.edu.cn (F. Du).

Content

1. Dialysis process	S2
2. Molecular dynamics simulations	S3
3. Loading capacity of FP-loaded nanocarriers	S4
4. Kinetic model fitting for the release process of FP-loaded nanocarriers	S6
5. Interface behavior experiment	S7
6. Significance analysis of plant height inhibition rate	S8
7. References	S9

1. Dialysis process

FP and FF were dissolved in EtOH at a concentration of 0.05 mol/L, respectively. Then the obtained solutions were mixed in a volume of 30 mL, respectively. And deionized water of 20 mL was added drop by drop. Subsequently, the solutions were placed in dialysis bags (MW 500) to dialyze against deionized water for 24 h (water was changed every 6 h). During the process, we tested the concentration of FP and FF in the external phase using HPLC with samples taken every 2 h. At the same time, 1 mL of deionized water was added to the external phase after each 1 mL sample, in order to ensure a certain total volume for each sample. The parameters of the HPLC are as follows: The mobile phases were methyl alcohol and water (v/v = 90:10) with a flow rate of 0.80 mL/min. The column temperature was kept at 25 °C. The injection volume was 10 μ L. The detection wavelengths were set as 210 nm when detect FP and as 200 nm when detect FF.

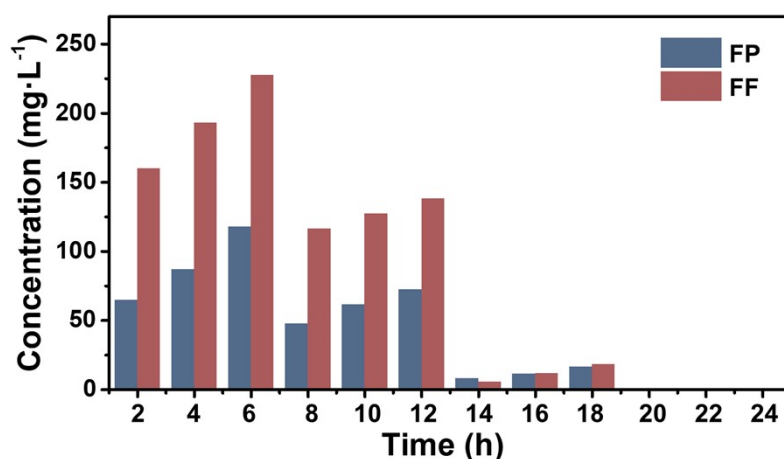


Figure S1. Concentration changes of FP and FF in the external phase with time during dialysis.

2. Molecular dynamics simulations

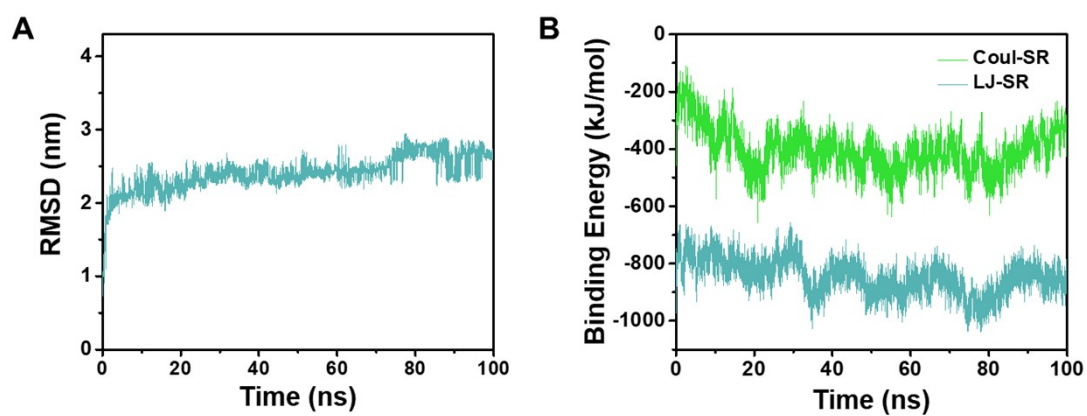


Figure S2. Co-assembly molecular dynamics simulations of FP and FF. (A) Root-mean-square deviation (RMSD) of all atoms in the system as a function of simulation time. (B) Variation of intermolecular binding energy in FP/FF system with simulation time.

3. Loading capacity of FP-loaded nanocarriers

Ratio of FP/FF	1:2	1:1	2:1
Theoretical Loading Capacity (%)	28.99	44.90	62.02
Experimental Loading Capacity (%)	49.96	61.68	72.34

Table S1. Loading capacity (LC) of FP-loaded nanocarriers.

Reference	Loading target	Construction strategy	Loading capability	Functionality
1	lambda-cyhalothrin	microemulsion polymerization nanogels	18.3%	temperature-responsive release, good pyrolysis resistance, upward translocation
2	prothioconazole	amphiphilic polymers assembled nano-micelle	20.6%	pH-responsive release, long-term antifungal properties
3	azoxystrobin	surface modification of mesoporous silica nanoparticles with carboxymethyl chitosan	21.0%	pH-responsive release
4	prochloraz	one-step esterification reaction	24.0%	prolonging retention and flush resistance on foliage
5	spinosad	polylactic acid encapsulated mesoporous silica nanoparticles	38.6%	improved photostability, intestinal microenvironment-responsive release
This work	fluroxypyr	supramolecular co-assembly	49.96% (1:2 system) 61.68% (1:1 system) 72.34% (2:1 system)	pH-responsive release

Table S2. Comparison between this work and conventional pesticide carriers.

4. Kinetic model fitting for the release process of FP-loaded nanocarriers

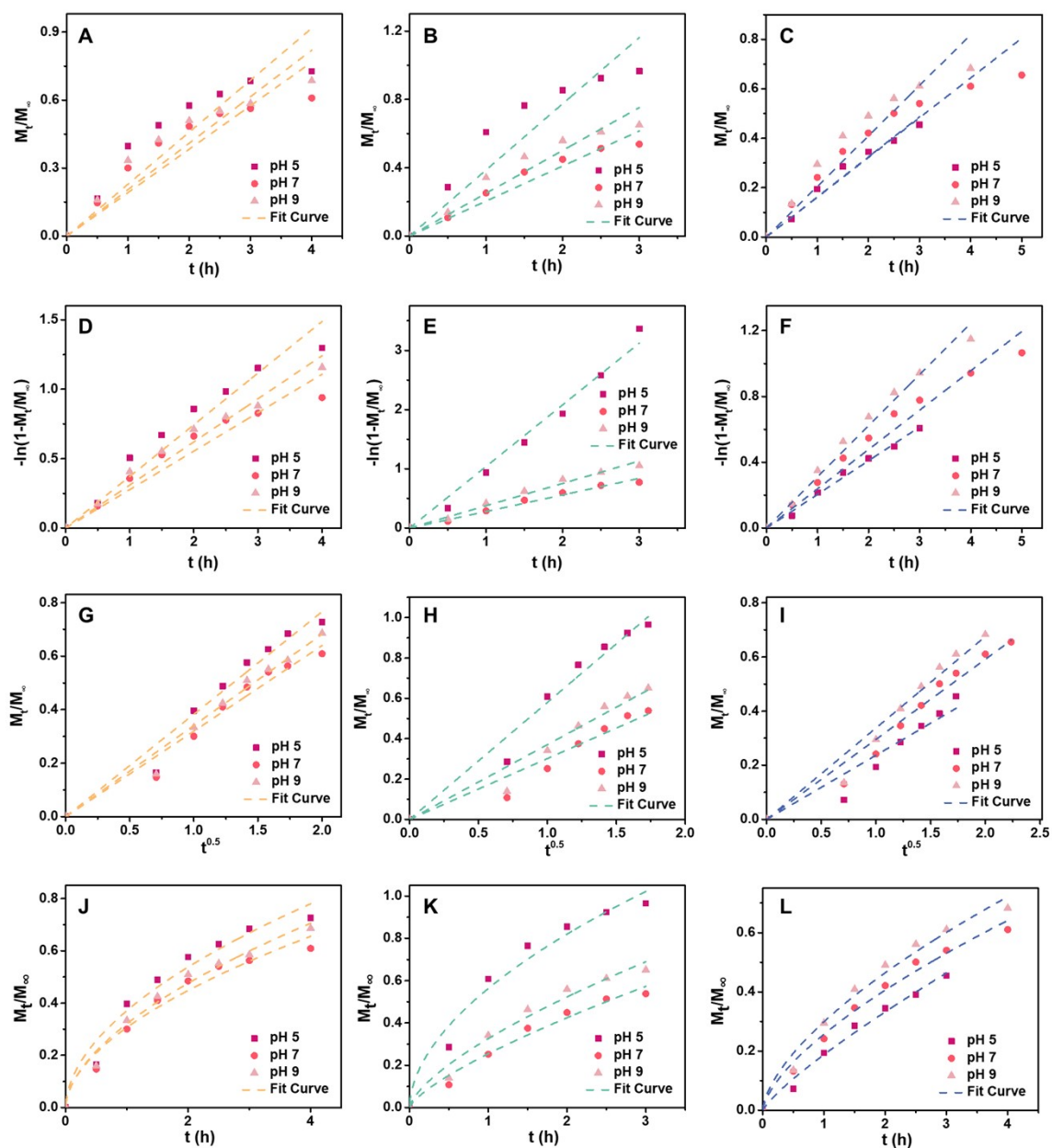


Figure S3. Fitted release curves of FP-loaded nanocarriers in different FP/FF ratios of 1:2 (A, D, G, J), 1:1 (B, E, H, K), 2:1 (C, F, I, L) under different pH values using zero-order model (A-C), first-order model (D-F), Higuchi model (G-I) and Ritger-Peppas model (J-L).

5. Interface behavior experiment

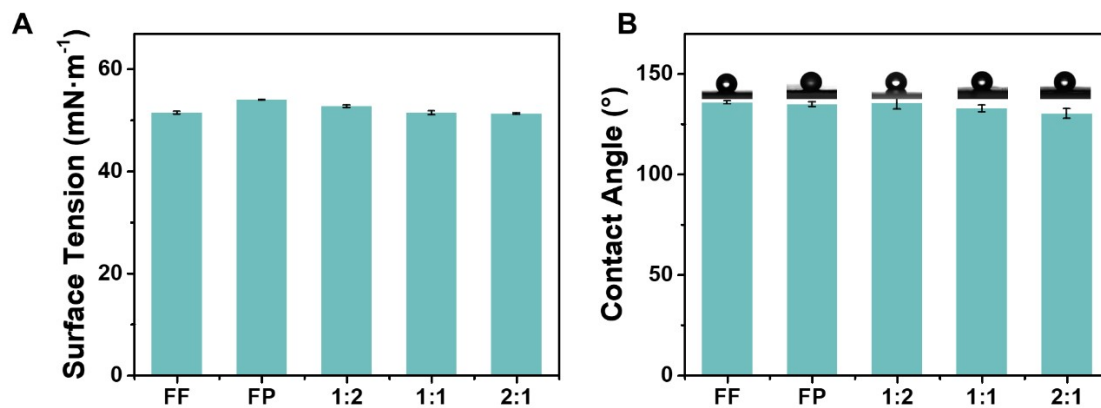


Figure S4. Interface behavior of FF, FP and FP/FF co-assembled suspensions. (A) Surface tension. (B) Contact angle on PTFE surface.

6. Significance analysis of plant height inhibition rate

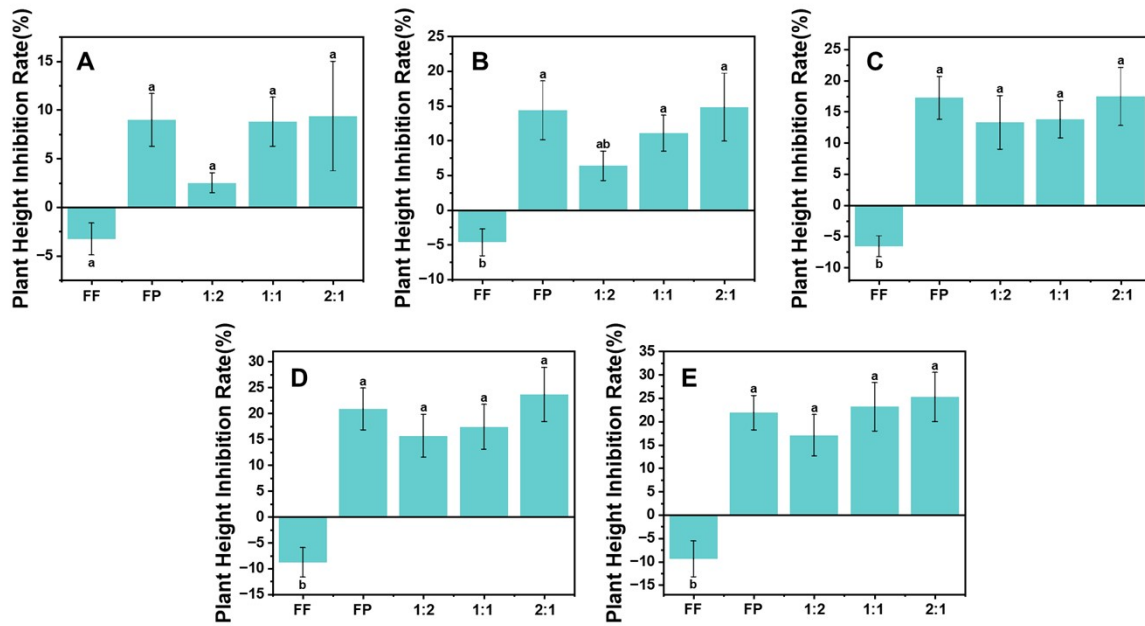


Figure S5. Plant height inhibition rate after treatments for 1 (A), 4 (B), 7 (C), 10 (D) and 14 (E) days. Different lowercase letters indicate significant differences between treatments ($p < 0.05$), Tukey test was used for multiple group analysis.

7. References

- [1] T. Wu, K. Zhao, S. Liu, Z. Bao, C. Zhang, Y. Wu, R. Song, Y. Gu, Y. Gao and F. Du, Promising nanocarriers endowing non-systemic pesticides with upward translocation ability and microbial community enrichment effects in soil, *Chem. Eng. J.*, 2023, **474**, 145570.
- [2] C. He, T. Wu, J. Li, X. Zhang, Z. Zheng, Y. Gao, C. Zhang, T. Zhong, Y. Zhang and F. Du, Bio-stimulant based nanodelivery system for pesticides with high adhesion and growth stimulation, *Chem. Eng. J.*, 2024, **491**, 151904.
- [3] C. Xu, L. Cao, P. Zhao, Z. Zhou, C. Cao, F. Li and Q. Huang, Emulsion-based synchronous pesticide encapsulation and surface modification of mesoporous silica nanoparticles with carboxymethyl chitosan for controlled azoxystrobin release, *Chem. Eng. J.*, 2018, **348**, 244-254.
- [4] K. Zhao, B. Wang, C. Zhang, Y. Guo, Y. Ma, Z. Li, T. Wu, Z. Bao, Y. Gao and F. Du, Catechol functionalized hat-shape carriers for prolonging pesticide retention and flush resistance on foliage, *Chem. Eng. J.*, 2021, **420**, 127689.
- [5] C. Wang, K. Qiao, Y. Ding, Y. Liu, J. Niu and H. Cao, Enhanced control efficacy of spinosad on corn borer using polylactic acid encapsulated mesoporous silica nanoparticles as a smart delivery system, *Int. J. Biol. Macromol.*, 2023, **253**, 126425.